IAEA
INTERNATIONAL ATOMIC ENERGY AGENCY

21st IAEA Fusion Energy Conference

Chengdu, China, 16-21 Oct 2004

IAEA-CN-149 / TH / 1-1

Studies of the Tokamak Edge with Self Consistent Turbulence, Equilibrium, and Flows

B. Scott[1], A. Kendl[2], D. Reiser[3], T. Ribeiro[4], and D. Strintzi[1]

[1]Max-Planck-Institut für Plasmaphysik, EURATOM Association, D-85748 Garching
[2]Institut fuer theoretische Physik, University of Innsbruck, Innsbruck, Austria
[3]Institut für Plasmaphysik, FZ-Jülich, EURATOM Association
[4]CFN-IST, University of Lisbon, Lisbon, Portugal

Studies of the Tokamak Edge with Self Consistent Turbulence, Equilibrium, and Flows

B. Scott[1], A. Kendl[2], D. Reiser[3], T. Ribeiro[4], and D. Strintzi[1]

[1]Max-Planck-Institut für Plasmaphysik, EURATOM Association, D-85748 Garching
[2]Institut fuer theoretische Physik, University of Innsbruck, Innsbruck, Austria
[3]Institut für Plasmaphysik, FZ-Jülich, EURATOM Association
[4]CFN-IST, University of Lisbon, Lisbon, Portugal
e-mail: bruce.scott@ipp.mpg.de

Abstract We report on gyrofluid and gyrokinetic numerical studies of edge and core turbulence in tokamak geometry, with emphasis on the self consistent interaction with the equilibrium and with large scale magnetic disturbances imposed externally. Computations driven by a set of fixed sources show naturally occurring global bursts associated with breakdown of the poloidal/toroidal flow equilibrium when the transport through the layer overcomes the geodesic equilibrium timescale. The E-cross-B flows in quiescent phases are determined by the same diamagnetic compression processes which give the neoclassical balances. Similar computations at ideal unstable parameters show a violent collapse of the profiles, nevertheless without an explosive nonlinear instability.

1. Physical Situation of the Tokamak Edge

The tokamak edge is defined by parameters: scale ratios are more important than collisionality [1]. The profile scale (nominal temperature scale length) $L_\perp$ is so much smaller than the minor and major radii a and R that the normalised mass ratio $\hat{\mu} = (m_e/M_i)(qR/L_\perp)^2 > 1$, and hence parallel electron dynamics always has a central role. The adiabatic response between parallel electron pressure and electrostatic potential gradients, mediated by currents, is always able to impose a character similar to ion temperature gradient (ITG) turbulence similar to the tokamak core even though the electron energetics is very robust. The ITG character results from the relatively shallow density gradient. Logarithmic gradient ratios $\eta = d\log T/d\log n$ are close to 2 in both species [2,3]. Due to the steep gradient the local drift parameter $\rho_s/L_\perp$ is nearly never smaller than 10^{-2} in the closed field line edge regions. The situation is usually transcollisional for the electrons, as $\hat{\nu} = \nu_e L_\perp/c_s \sim 1$, while for ions the collisionality is weak enough, $\nu_i < c_s/R$, that time dependent perturbations even in the equilibrium are outside the validity of collisional fluid equations. In terms of turbulence, the vorticity spectrum always extends to $k_\perp \rho_i \sim 1$, so that failure to resolve this range would injure ability to capture the turbulence with convergent computations. In modern tokamaks the edge pressure is large enough to make the drift Alfvén parameter $\hat{\beta} = (4\pi p_e/B^2)(qR/L_\perp)^2$ also larger than unity, so that the drift wave physics becomes electromagnetic. These features together all lead one to expect a robust physical situation in which none of the familiar restrictive limits (linearity, electrostatic adiabatic electrons, or even MHD) are applicable.

The following were all run within the GEM (Gyrofluid ElectroMagnetic) model, unless otherwise indicated (see Secs. 3,4, below). GEM is described in Ref. [4], with a simplified discussion in terms of the salient parameters also given in Ref. [5]. It is a six moment gyrofluid model following Refs. [6,7], with electromagnetic electron dynamics added in Ref. [8] and corrected for free energy conservation in Ref. [4]. The methods for treating the self consistent equilibrium are given in Ref. [9].

2. Parameter Scaling, Zonal Flow Energetics and Effects of Shaping

The basic scaling of edge turbulence with inductivity ("beta," $\hat{\beta}$) and collisionality ($C = 0.51\hat{\mu}\hat{\nu}$) was revisited, along with the effects of magnetic flux surface shaping [10]. The scaling results are in agreement with the end of the first wave of 3D edge turbulence computation

[8,11–13], and in contrast to earlier results [14] which became the basis for local instability based L-to-H Mode transition modelling [15,16]. The current state of the art (for the parameter regimes and requirements for computations see Ref. [5]) is that the transport is insensitive to beta until the transition to ideal ballooning sets in. The ideal and resistive ballooning transitions, which are opposite to the L-to-H requirements, are detailed in Ref. [17]. The ideal transition involves a long wavelength mode ($k_\perp \rho_s < 0.1$) which is at least partially driven nonlinearly. Its scale does not follow from the underlying linear theory. Earlier computations which imposed radial and electron-drift periodicity in a 1×1 computational domain excluded this mode. Diagnosis of the transition via relative phase shifts among the fluctuations show that the longest wavelengths always change first, also in contrast to linear theory. The reason for the weakness of the dominant short wavelength linear instabilities in turbulence is that their growth rates are below the corresponding diamagnetic frequencies ($\omega_* = cT_e k_\perp / eBL_\perp$) and hence they are shear-stabilised by the native vorticity of the drift wave turbulence [17].

The first wave of computations up to 1999 usually considered equal gradients, $\eta = 1$ in all species, for models including the temperature dynamics. The character is either ballooning or drift wave like depending on $\hat{\beta}$ and C. For $1 < \eta < 2$ there is a smooth transition to ITG character in both the linear modes [18] and, as measured by mode structure diagnostics, the turbulence [19,17]. For $\eta = 2$ the structure is decidedly ITG like, with $\widetilde{T_i}/T_i$ the largest and most ballooned fluctuation, and with $e\widetilde{\phi}/T_e$ similar to and phased close to $\widetilde{p_e}/p_e$, and with the difference between these two the least ballooned ("flat"). In addition, the finite $\hat{\beta}$ tends to make $e\widetilde{\phi}/T_e$ itself flat, a clear shear Alfvén signature. The basic character is much closer to core ITG turbulence than to the results of pure-MHD resistive-G models (control tested in Ref. [17]).

This also affects zonal flow energetics. Both core ITG and edge drift wave turbulence show pronounced positive Reynolds stress drive to the flows, with the geodesic curvature (ExB toroidal compression) providing energy transfer to the poloidally asymmetric ("sideband") pressure component [20–23]. Artificial variation of the geodesic coupling strength shows a clear inverse scaling with the transport [24]. Edge ITG turbulence however includes three elements whose combination is found to eliminate the Reynolds stress drive: $\eta_i = 2$, finite $\hat{\beta} > 1$, and strongly nonadiabatic electron dynamics. Slab geometry control tests run in the manner of Ref. [23] show a Reynolds stress drive level statistically not different from zero. The process controlling the flows becomes neoclassical response to quasilinear changes in the zonal pressure, with diamagnetic flow compression providing the transfer channel. This is why our self consistent equilibrium cases show essential neoclassical flow divergence and parallel force balances unless the turbulence produces a global burst (see below). This finding is consistent with recent edge modelling studies which, including only the neoclassical flow drift and parallel compression processes but no turbulence, find electric field profiles consistent with observations [3].

Flux surface shaping enters mainly by changing the local magnetic shear values: the shear is weaker on the outboard side of the torus but is very strong on top and bottom, stronger with elongation. The result is a sharp inverse scaling with ellipticity but a weak effect due to triangularity [10]. The local shear effect itself was studied earlier, including the effect of proximity to the X-point [25]. Ultimately, ellipticity by itself is sufficient to shorten the effective field line length, de-emphasising the basic ITG strength at longer wavelength.

3. Effects of an Ergodic Magnetic Boundary

The reaction of the turbulence to the presence of an externally applied ergodic magnetic field layer was studied within the basic four-field edge turbulence model by means of control tests at moderate and very high collisionality [26]. Chirikov parameters below and above unity were considered. The entire flux surface is computed because of the low order helicity of the perturbations; resolving the ion gyroradius scale as usual yields a large domain in the drift-angle

direction. Typically, 1024 grid nodes are carried in the toroidal angle (the method of including the ergodic perturbations into the field aligned coordinates of Ref. [27] is detailed in Sec. II.C of Ref. [26]). This separation of scales, not demonstrated on this problem before, leads to a complicated, indirect reaction of the turbulence. Due to the self consistent current effect there is little direct parallel magnetic transport. However, the large scale perturbation leads to a corresponding change in the time-independent gradient distribution; effectively, a 3-D equilibrium. The applied radial magnetic field component leads to stronger ExB transport in weakly collisional cases.

4. Turbulence on Open and Closed Field Lines, and the Self Consistent Equilibrium

A set of Debye sheath boundary conditions was constructed for the GEM code in Ref. [28]. At the sheath, located between two parallel grid nodes, the state variables ($\widetilde{\phi}$ and densities and temperatures) are given Neumann conditions and the flux variables (parallel flows and heat fluxes hence including the current) are given Dirichlet conditions in terms of the state variables. This allows treating the edge (closed) and SOL (open field lines) separately or together. The control case is to run each separately at the same basic parameter set and examine the effect of the Debye boundary conditions. The effect, much larger than results from parameter changes, is to allow pure flute modes ($k_{\|} = 0$ with $k_{\perp} \neq 0$ in the wavenumbers) in the SOL. These have interchange dynamics, in contrast to the ITG (or in a four-field model, drift wave) dynamics in the edge. Debye sheath coupling between $\widetilde{\phi}$ and the other state variables was found to affect mainly the profiles. This sets the $\widetilde{\phi}$ profile in the SOL, precluding the zonal flow physics found on closed magnetic surfaces.

The SOL necessitates treating the equilibrium self consistently, as the dynamics there is so powerful that saturation with fixed gradients in local fluxtube models is not achieved. The contrast in the set-up between local and global models within the same set of equations is detailed in Ref. [4]. The main new ingredient is that the geodesic curvature acts upon the background profiles, producing diamagnetic flow divergences. Consequently, the parallel Pfirsch-Schlüter flows and currents develop to balance the divergences (parallel divergences in the flux variables balancing geodesic compression terms in every equation). As all of the flow divergence and parallel force balances in all the sideband components become maintained, the profile of the electrostatic potential is determined by the gyrocenter densities (the polarisation equation). This is the essential 2D neoclassical equilibrium, reffered to as such even though the steep gradients place the edge well outside of the usual neoclassical scale ordering. Indeed, this is seen in the contrast in scale separation between typical edge and core cases as shown in Ref. [9]. Note this does not mean simple "radial force balance" as typically there is a radial force imbalance leading to a net geodesic compression (ExB plus diamagnetic in the flows) which is then made up by a parallel flow residual which is significant in the core but small in the edge (since $\rho_s/L_{\perp} > L_{\perp}/qR$ and $q > 1$).

These general balances naturally extend to the currents. The Pfirsch-Schlüter current and hence the Shafranov shift become part of the dynamics. One has to be careful not to double count the latter – if the shift is included in the metric it must be taken out of the magnetic potential variable $A_{\|}$ and vice versa. The method to do this is given in Ref. [9]. This sideband component of the MHD equilibrium is not in fact assumed to be in equilibirum; the Shafranov shift is found from the sideband current, not the pressure gradient. Indeed the abovementioned zonal flow energetics studies have found that significant zonal flow energy is dumped into the sideband current and dissipated resistively [23].

The physics of this coupling to the MHD equilibrium involves the "global geodesic Alfvén oscillation" which is the transient response to an initialised 1D equilibrium pressure profile. The end state is the Pfirsch-Schlüter current in quasistatic equilibrium. Computationally, however,

this oscillation is a required element for electromagnetic turbulence; the code must be stable to it and represent its damping properly. This transient is shown in Refs. [9] and [29].

The turbulence itself shows a relatively sharp transition across the last closed flux surface (LCFS), between ITG mode structure in the edge and interchange structure in the SOL. The transition width is of order $10\rho_s$ [9]. When the equilibrium density and temperature profiles are fixed at both ends, or (better) maintained by a set of fixed sources at the innermost radial boundary, the turbulence is well saturated and the equilibrium is relatively well formed although the neoclassical balances show equlibrium only when time averaged over several tens of gyro-Bohm ($L_\perp/c_s$) times. However, for higher levels of the fixed sources the equilibrium quasi-periodically breaks down and there are large global bursts, which we address in the following Section.

5. Global Bursts in the Self Consistent Equilibrium

Bursts in turbulence and turbulent transport are of recent interest, motivated by the observation of Edge Localised Modes (ELMs [30]) in tokamaks. Most often described in terms of relaxation phenomena, they appear to result when the pressure gradient reaches some threshold. It is imagined that a new linear instability arises, its threhsold having been surpassed, but the observations do not distinguish this from the mere reappearance of the turbulence out of its suppression during the H-Mode state.

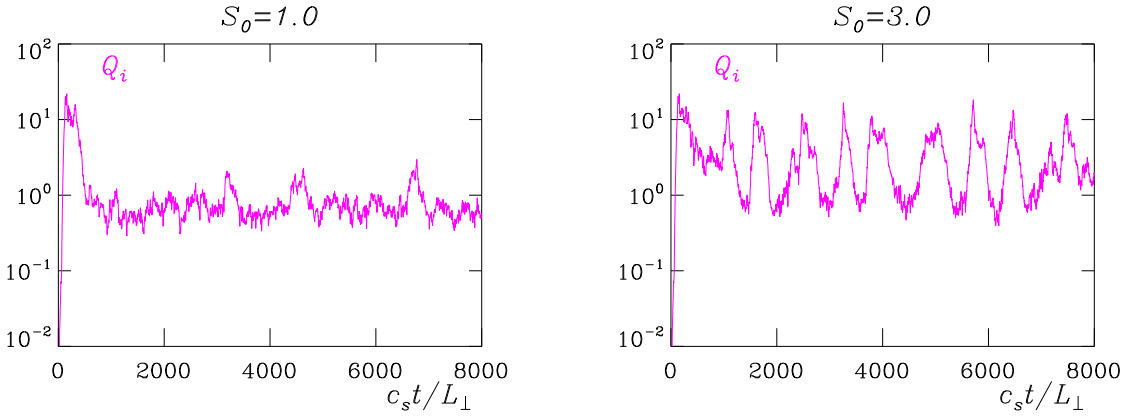

FIG. 1: Bursty turbulence for moderate edge turbulence (left) compared to global burst events (right) for larger heat source drive levels. The ion heat fluxes in terms of $p_i c_s(\rho_s/L_\perp)^2$ are plotted; the curves for the electron heat and particle fluxes are similar.

These computations have so far not reproduced the H-Mode (though false positives are often reported), but there is recent interest their burst phenomenology nevertheless. Bursts can occur in the turbulence when caused by dissipation (not enough degrees of freedom), or when the zonal E-cross-B vorticity layer is artificially forced with a time delay in response to the zonal pressure gradient. However, these models, which are either two dimensional or lacking the geodesic curvature effects which produce the zonal flow equilibrium, do not treat the toroidal flow equilibrium self consistently, even the perturbed equilibrium resulting from radially localised zonal perssure fluctuations. They may or may not treat an layer of sheared zonal E-cross-B flow, but without the geodesic curvature effects the treatment is forced to be artificial. When the turbulence is run with resolution down to the ion gyroradius scale, and the non-MHD processes are followed, the resulting dynamical system is relatively weakly dissipative and involves many degrees of freedom. A two-moment gyrofluid model equivalent to a standard four field fluid model in the manner explained in Ref. [5], run with a fixed source maintaining the zonal profile which in turn drives the turbulence, did not find global burst phenomena at any

level of the source drive, or at any level of $\hat{\beta}$ or C [29]. The turbulence changed character into resistive or ideal ballooning for $\hat{\beta}(2L_\perp/R) > 1$ or $C(2L_\perp/R) > 1$ as detailed in Ref. [17], but the burstiness remained that intrinsic to the turbulence: transport varying within a factor of two or so with much of the transport in the stronger events, but always with the same mode structure character (as diagnosed, e.g., in Refs. [5,8,17,19]). Since the possibility of momentary spectral migration (e.g., broadening or narrowing, or shifting of the peak in terms of $k_y\rho_s$) of any process was allowed, confinement transitions or global bursting effects resulting solely from the turbulence were not found (hence the importance of the abovementioned computational considerations). The status of this is covered in Refs. [5,8,9,19].

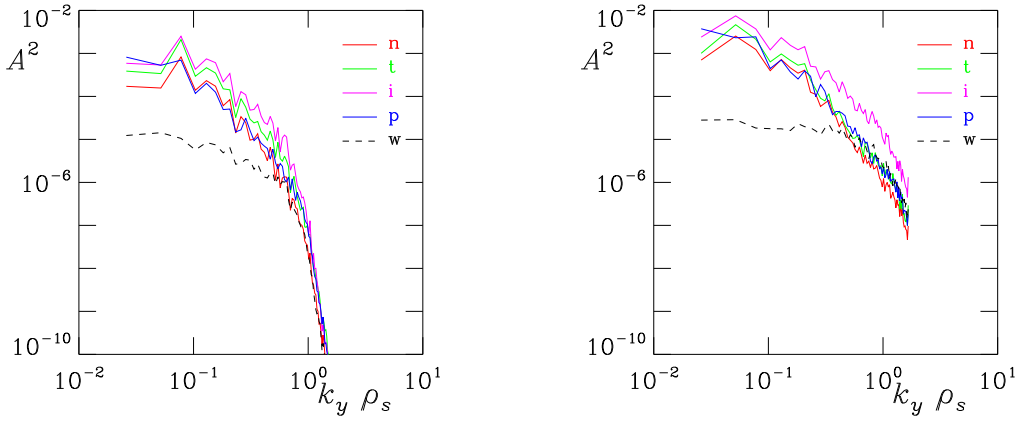

FIG. 2: Fluctuation amplitude spectra in the phases between (left, $c_s t/L_\perp = 2000$) and during (right, $c_s t/L_\perp = 5000$) global bursts for $S_0 = 3.0$. From top to bottom at $k_y\rho_s = 0.1$ they are ion and electron temperatures (i and t), density (n), potential (p), and vorticity (w) in both cases. The shapes of the spectra for $k_y\rho_s < 1$ do not change during the bursts; the level of nonadiabatic activity merely increases.

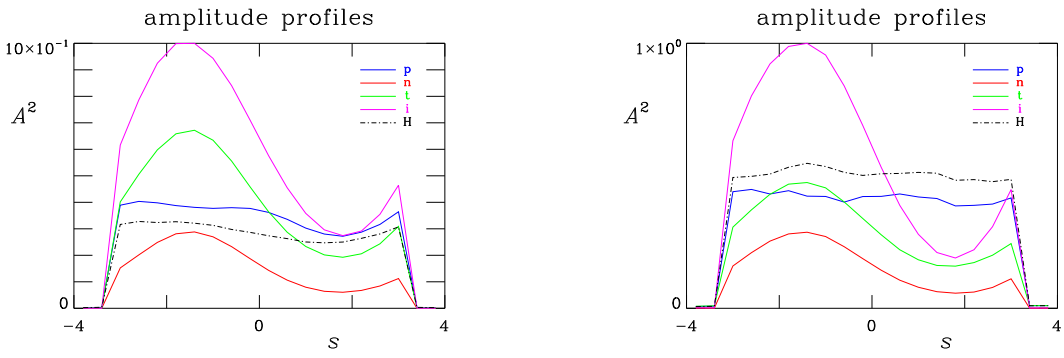

FIG. 3: Fluctuation amplitude parallel envelopes in the phases between (left, $c_s t/L_\perp = 2000$) and during (right, $c_s t/L_\perp = 5000$) global bursts for $S_0 = 3.0$. From top to bottom at $s = -\pi/2$ (outboard midplane) they are ion and electron temperatures (i and t), potential (p), nonadiabatic density (H), and density (n) in the left frame, and i, H, t, p, and n in order in the right frame. The envelope shapes do not change during the bursts; the level of nonadiabatic activity merely increases.

On the other hand, global burst phenomena have been found in computational tokamak edge

turbulence in cases where (1) the profile situation is in the ion temperature gradient (ITG) regime, with $\eta = 2$ [2], and (2) the equilibrium is carried self consistently. The scenario is that of Ref. [9], with parameters

$$T_e = T_i = 100\,\mathrm{eV} \qquad n_e = n_i = 2.0\times 10^{13}\,\mathrm{cm}^{-3} \qquad B = 2.5\,\mathrm{T}$$
$$R = 165\,\mathrm{cm} \qquad L_T = L_\perp = 3.5\,\mathrm{cm} \qquad L_n = 7.0\,\mathrm{cm} \qquad q = 3.5 \qquad \hat{s} = 1.14 \qquad (1)$$

This case has $\hat{\beta} = 1.75$ and $\hat{\mu} = 7.41$ and $C = 3.11$ and $2L_\perp/R = 0.0424$ in terms of local parameters. The geometry treats both the closed and open flux surface regions with separatrix topology, with a domain of 3.5 cm on either side of the separatrix. The sense of the s coordinate is changed such that $s = 0$ corresponds to the top of the torus, with $s = -\pi/2$ the outboard midplane. Hence $\sin\theta$ corresponds to $\cos s$. The additional proviso is a fixed source for particles and energy: the densities and temperatures are maintained in the manner given in Ref. [29].

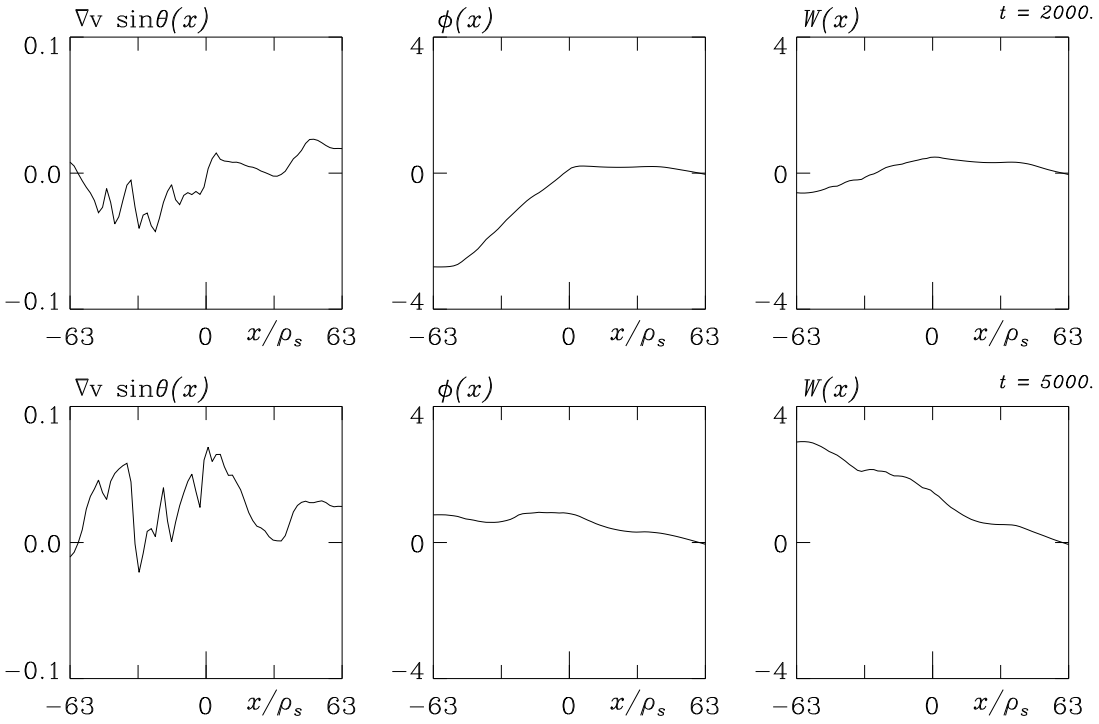

FIG. 4: Profiles of the sideband ion flow divergence, electrostatic potential, and ion force potential (W) in the phases between (top, $c_s t/L_\perp = 2000$) and during (bottom, $c_s t/L_\perp = 5000$) global bursts for $S_0 = 3.0$. The flow is close to a slowly growing equilibrium state between bursts. During a burst, the flow equilibrium breaks down, leaving the turbulence intrinsically stronger in the absence of the flow shear layer. About one third of the total energy in the profile has been lost during the burst.

For moderate source levels, a gradient in the range of $1.0 - 1.2 \times T_e/L_\perp$ is produced, with a well formed ion flow equilibrium and bursty turbulence with an E-cross-B energy transport level in the range of $0.5 - 1.0 \times p_e c_s(\rho_s/L_\perp)^2$. For larger source levels much more pronounced global bursts are found. Correpsonding time traces of the ion heat flux are shown in Fig. 1 for two such drive levels. However, these are not due to the appearance of a new instability, just the intrinsic turbulence at a higher level. Both the spectra (Fig. 2) and parallel envelopes (Fig. 3) of the fluctuation amplitudes are unchanged in shape, just the nonadiabaticity of the electrons is stronger. It is the sideband ion flow divergences and electrostatic and ion force potential profiles

that show the strong changes. These are in Fig. 4. The flow divergence is close to zero between bursts, showing a slowly evolving equilibrium over medium time and radial space scales, with W and $\nabla \cdot \mathbf{v}$ near zero. During the burst phases the flow equilibrium breaks down entirely, with W well above zero and the shear layer in ϕ destroyed. The intrinsic transport ability of the turbulence has overcome the equilibration time scales of the ions (near $2\pi R/c_s$), at which point the flow dynamics cannot maintain the equilibrium in the presence of the turbulence. Obviously, if the geodesic curvature effects were not represented, then the flow equilibration physics could not be followed, and bursts of this type could not be studied.

5.1. Ideal Ballooning Mode Blowout Studies A separate scenario is being applied elsewhere to ELMs: An H-Mode set of profiles is initialised with small fluctuations whose growth according to ideal ballooning mode (IBM) instability is then followed [31]. Nonlinear ballooning theory, which by convention neglects such things as poloidal periodicity, predicts epxlosive nonlinear growth, with the inferred growth rate reaching singularity in finite time [32]. Whether this is actually be a consistent scenario for ELMs is one thing, but whether it actually occurs for a model IBM Blowout computation is another. The result published in Ref. [31] bears several similarities with numerical difficulties associated with strong, transient nonlinearity.

Transition to turbulence from initial instabilities was studied in detail in Ref. [17]. As the most unstable linear modes crystallise out of an initial random bath of small-amplitude perturbations, the linear growth rate rises and becomes steady. The maximum value of the instantaneous growth rate given by $\Gamma = (2E)^{-1}\partial E/\partial t$ may be taken as the maximal linear growth rate. The curve of $\Gamma(t)$ then falls very sharply to zero (over about $10L_\perp/c_s$) as saturation occurs. There is some structural adjustment over the next few $100L_\perp/c_s$ as the spectrum fills out, and then the turbulence is fully developed. But over the adjustment phase the value of Γ is well below its previous maximum.

The IBM Blowout scenario is similar to this, initially, except that the instability is not a microinstability. Nevertheless, the scale differs by less than an order of magnitude (the resistive linear toroidal mode numbers are in the range of $50-100$ while the main IBM is near mode number 10, on the entire flux surface, for these typical $\rho_s/L_\perp$ values). The profiles used here come from Ref. [3]. There is no need to enhance the gradient value since the mechanism for the H-Mode itself is lacking. The entire flux surface is carried, with a radial range equal to $L_\perp$ on either side of the LCFS. The radial/toroidal grid is 64×512 (perpendicular node spacings below ρ_i) and the parallel/poloidal domain is given 16 nodes as usual. The parameters are

$$\begin{array}{lllll} T_e = 300\,\mathrm{eV} & T_i = 360\,\mathrm{eV} & n_e = n_i = 2.5\times 10^{13}\,\mathrm{cm}^{-3} & B = 2.0\,\mathrm{T} & \\ R = 165\,\mathrm{cm} & L_T = L_\perp = 3.0\,\mathrm{cm} & L_n = 6.0\,\mathrm{cm} & q = 5.0 & \hat{s} = 1.5 \end{array} \qquad (2)$$

yielding extreme values $\hat{\beta} = 28.5$ and $L_\perp/\rho_s = 24$ (only). The 2D equilibrium is evolved to stationarity before the turbulence is initialised with the usual random bath (cf. Ref. [27]) for $\widetilde{n}_e = \widetilde{n}_i$ at relative amplitude $10^{-10}\rho_s/L_\perp$. The instability is very violent, growing at a rate $0.18c_s/L_\perp$, just below the ideal interchange rate. The subsequent growth curve $\Gamma(t)$ appears qualitatively like the basic turbulence ones, however, except for several overshoot oscillations at saturation. At all time points in the nonlinear phase $\Gamma(t)$ is well below its previous maximum at $0.18c_s/L_\perp$. At late times the initial blowout no longer imprints the results – with a fixed source one merely finds bursty turbulence thereafter. Hence, there is no evidence for explosive instability. The presence or absence of background current gradient terms ($\widetilde{J}_\parallel \to \widetilde{J}_\parallel + J_0$ everywhere the electron $\widetilde{v}_\parallel$ appears in the equations, with J_0 given by the q profile) was found to have no discernable effect on the result (since in physical units J_0 is well below $n_e e c_s q R/L_\perp$).

One will have to investigate further than this to find the physical mechanism behind the H-Mode and ELMs. The important things which have been learned in any case are: (1) dynamics

down to the ion gyroradius scale do enter even for these cases, (2) linear character does not necessarily control the overall dynamics and realistic scenarios can be constructed without new instabilities, (3) computations must not be constructed around particular types of modes, but should always include the entire range from the global scale down to ρ_i. In particular, it should be understood that assumptions that wide-spectrum nonlinearity, and/or that the ion gyroradius do not enter, should be avoided.

6. Progress in Nonlocal Gyrofluid and Gyrokinetic Computation

Nonlinear, nonlocal gyrofluid equations were derived using Lagrangian field theory methods, for an anisotropic pressure [33]. The same energy transfer pathways as in the GEM equations are present. A general method for insertion of dynamical and diamagnetic heat fluxes has been found which preserves exact energy conservation to all orders in the gyroradius. The particular expressions are determined by correspondence with Ref. [4], which is in turn has a derivation from the delta-f gyrokinetic equation via moments. Construction of the descendant nonlocal nonlinear electromagnetic gyrofluid computations is underway. Turbulence in the self consistent equilibrium (this model cannot be done any other way) is being studied in the context of the nonlocal version of Ref. [29], i.e., the isothermal two-moment version. Global geodesic Alfvén oscillations behave normally. The six-moment version is the minimal one, however, for studies corresponding to the above H-Mode and ELM scenarios, including the dynamical edge/core interaction.

A companion phase-space gyrokinetic model, also using field theory methods [34], is also under construction. This one is analogous to efforts elsewhere (cf. paper TH/P6-23 by X. Q. Xu, this conference). Problems are still encountered in the global geodesic Alfvén oscillations however. It is well represented for about five Alfvén periods but then becomes unstable at short parallel wavelength. Subtle interactions between the numerics and the Hamiltionan nature of the kinetic system are involved, and the solution is still sought. One other major problem not faced yet is the difficulty of representing a strongly inhomogeneous temperature coupled to the need to resolve velocity space, not least for collisions. It may become necessary to have a time-dependently adaptive velocity space grid, which would make the resolution demands of the scenarios described above unattainable until the next generation of computational resources becomes available.

References

[1] SCOTT, B., Plasma Phys. Contr. Fusion **39** (1997) 1635.
[2] NEUHAUSER, J. et al., Plasma Phys. Contr. Fusion **44** (2002) 855.
[3] HORTON, L. D. et al., Plasma Phys. Contr. Fusion **45** (2005) 856.
[4] SCOTT, B., Phys. Plasmas **12** (2005) 102307.
[5] SCOTT, B., Plasma Phys. Contr. Fusion **45** (2003) A385.
[6] DORLAND, W. et al., Phys. Fluids B **5** (1993) 812.
[7] BEER, M. et al., Phys. Plasmas **3** (1996) 4046.
[8] SCOTT, B., Phys. Plasmas **7** (2000) 1845.
[9] SCOTT, B., Contrib. Plasma Phys. **46** (2006) 714.
[10] KENDL, A. et al., Phys. Plasmas **13** (2006) 012504.
[11] NIEDNER, S. et al., Plasma Phys. Contr. Fusion **44** (2002) 397.
[12] NAULIN, V., New J. Phys. **4** (2002) 28.
[13] NAULIN, V., Phys. Plasmas **10** (2003) 4016.
[14] ROGERS, B. N. et al., Phys. Rev. Lett. **81** (1998) 4396.
[15] GUZDAR, P. N. et al., Phys. Plasmas **11** (2004) 1109.
[16] KALUPIN, D. et al., Nucl. Fusion **45** (2005) 468.
[17] SCOTT, B., Phys. Plasmas **12** (2005) 062314.
[18] ZEILER, A. et al., Plasma Phys. **5** (1998) 2654.
[19] SCOTT, B., New J. Phys. **4** (2002) 52.
[20] SCOTT, B., Phys. Lett. A **320** (2003) 53.
[21] MIYATO, N. et al., Phys. Plasmas **11** (2004) 5557.
[22] NAULIN, V. et al., Phys. Plasmas **12** (2005) 052515.
[23] SCOTT, B., New J. Phys. **7** (2005) 92.
[24] KENDL, A. et al., Phys. Plasmas **12** (2005) 064506.
[25] KENDL, A. et al., Phys. Rev. Lett. **90** (2003) 035006.
[26] REISER, D. et al., Phys. Plasmas **12** (2005) 122308.
[27] SCOTT, B., Phys. Plasmas **8** (2001) 447.
[28] RIBEIRO, T. et al., Phys. Plasmas **47** (2005) 1657.
[29] SCOTT, B., Phys. Plasmas **12** (2005) 082305.
[30] ZOHM, H., Plasma Phys. Contr. Fusion **38** (1996) 1213.
[31] SNYDER, P. et al., Phys. Plasmas **12** (2005) 056115.
[32] WILSON, H. R. et al., Phys. Rev. Lett. **92** (2004) 175006.
[33] STRINTZI, D. et al., Phys. Plasmas **12** (2005) 052517.
[34] SUGAMA, H., Phys. Plasmas **7** (2000) 466.